# Acoustically Powered Magnetic Microrobots for Cellular Manipulation

Fatma Ceren Kirmizitas<sup>1,2</sup>, Max Sokolich<sup>1</sup>, Jeffrey McNeill<sup>3</sup>, Austin Maaddi<sup>4</sup> and Sambeeta Das<sup>1</sup>

Abstract—A grand challenge in robotics, and the scientific community as a whole, is developing tools to determine the fate of singular micro- and nanoscale objects with a high level of precision and speed, particularly cells for biomedical applications. Despite the recent surge of activity in this area, there still does not exist a system that contains most of the practical components for carrying out many complex tasks, such as fast and precise motion, tunable speed, appropriate length scale, bioorthogonality, and high throughput in the form controlling many robots at one time. Here, we demonstrate these characteristics in the form of an acoustically powered microrobot steered by an applied magnetic field. The acoustic propulsion mechanism provides a variety of highly desirable features, such as high speed, precision, short-range attractive forces utilized as an end effector, and orthogonality in any liquid medium. The potential power of this approach is highlighted by cargo pickup and delivery to individual cells and also cellular manipulation. In this paper, we show that not only are acoustic microrobots bio-compatible, but can also be used for cellular manipulation and targeted delivery.

Index Terms—Microrobots, ultrasound, cellular manipulation, delivery

## I. INTRODUCTION

Currently, the field of robotics research is teeming with new advances that are pushing the capabilities of large-scale machines into the regime where fundamental tasks such as running [1], lifting [2], and fine motor skills [3] are becoming easier feats to overcome. However, despite their many imaginable applications in industrial and biomedical applications, there is a lack of practical robots on the nano- and microscale, that could carry out operations currently limited to expensive and difficult-to-use systems such as optical, magnetic, and acoustic tweezers. Drawing a similarity to large-scale corporate operations, there already exist nano-/microscopic barcodes [4] that could be used to identify desirable microscale objects, but there is no practical way to separate them individually in dense environments. An ideal microrobotic system would have the ability to carry out a variety of precise tasks, such as manipulation, fast motion with easy redirection, and selective control of multiple robots, while maintaining a high level of stability and autonomy in a variety of media, from nonpolar solvents to viscous, high-ionic strength aqueous liquids found in biology. Thereby, we reported the design and implementation of a technique for manipulating microscale objects via an acoustically powered, bubble-actuated, magnetically steerable microrobot [5]. The robot's versatile, precisely controlled

motion and relatively large force output make it an ideal system for studying various microscale systems and can be pushed into the regime of micropatterning and assembly by the use of a computer-controlled driver. Thus this system could be used as acoustically powered microrobots and even more interesting and practical for robotics applications, the acoustic microrobots can be steered by an applied magnetic field, allowing for fast, yet extremely precise motion in two dimensions, with the addition of a simple tail pushing this complex motion into the third dimension. The biggest advantage of our method is that short-range acoustic forces radiated from the bubble effectively behave as an end effector at slightly higher operating voltages, allowing the robot to grab and release objects, rather than just push. This approach is also experimentally simple and affordable, requiring only a ceramic disc transducer glued to a silicon wafer or glass slide, powered by a sinusoidal waveform generator in the 1 to 1.6 MHz range at less than 1-volt peak-to-peak (Vpp.) In this paper, we build upon our previous work on acoustic microrobots and demonstrate their applications to mammalian cellular manipulation and targeted payload delivery. In the presence of an acoustic field and magnetic field, the bullet-shaped microrobots could be navigated. To demonstrate cell targeting, manipulation, and cargo delivery, we use the Human Embryonic Kidney (HEK) cell line. Additionally, we successfully demonstrate the cargo release to the target HEK site by pulling polystyrene particles as cargo.

# II. MOTIVATION

In general, the field of biomedicine could benefit greatly from a versatile, selective, and quick mode of cellular manipulation and cargo delivery for a variety of applications and research [6], [7], [8]. From an engineering standpoint, the manipulation and relocation of cells could lead to understanding cell-cell communications, single-cell behavior, the development of artificial organ systems, and high-fidelity cell sorting, driving advancements in biotechnology and medicine. Additionally, biologists could selectively position and rotate cells to study advanced microscopy, intercellular communication pathways, differences in molecular recognition, and targeted delivery of different biomolecules [9], [10], [11], [12]. Given these advanced, potentially transformative applications, methods of manipulating single cell are of intense interest to biologists and roboticists alike. While optical and magnetic tweezers are incredibly effective systems for manipulating micro and nanoscale objects, their force output is low [13], [14]. Optical tweezers are relatively costly and difficult to assemble, moreover, direct single-cell manipulation typically

<sup>1,2,4</sup> The authors are with the Department of Mechanical Engineering<sup>1</sup>, and the Department of Animal and Food Sciences<sup>2</sup>, University of Delaware, Newark, DE 19716 USA (emails: ceren@udel.edu; sokolich@udel.edu; samdas@udel.edu.)

<sup>&</sup>lt;sup>3</sup> J. MCNeill is the Nano Initiative Postdoctoral Fellow at Columbia University, New York, USA (email: jm5750@columbia.edu)

damages and kills them [15]. Practically, these systems have been augmented such that the surfaces are functionalized with biochemicals that have targeted functionalities. For instance, colloids driven by magnetic transporters have been functionalized with antibodies to test binding affinity with inflammatory proteins [16]. Similarly, optical traps have been used to test Tcell receptor affinity [17]. In both cases, the microrobots have an integrated mechanochemical action which is used to assess cellular activity. Acoustic tweezers are simpler and easier to use than optical tweezers, and their force output is much higher, but the length scale of acoustic waves in water affords difficulty in trapping single, sub-10 micron objects in crowded environments [18], [19]. Thus, moving single cells to the target site, or delivering payloads precisely and efficiently is challenging, especially in highly concentrated systems. Along with these techniques, there also currently exist a variety of microscale robots, which can carry out only extremely simple tasks, as they are hard to control and typically run on magnetic actuation and chemical fuels, which limit their range and types of motion, as well as their use in many types of media [20], [21]. In many examples, the previously mentioned techniques are limited to niche fields and applications that would be difficult to translate to industrial or biomedical fields where a high level of precision and throughput are needed [22], [23]. To overcome these issues, many teams are focusing on perfecting methods for manipulating and interfacing with single mammalian cells without causing damage or changing the cell's morphology or chemistry. Dai et al. have shown that microbubbles can be generated and controlled optothermally, allowing them to quickly and efficiently manipulate a variety of microscale objects [24]. Wang et al. have demonstrated complex, even intracellular manipulation of cells via magnetic manipulation of microbeads [25] with a complex magnetic tweezer setup. Others have attempted to use acoustically actuated robots for biomedical applications [26], although motion is typically limited or requires high acoustic powers that could damage cells and generate undesirable bulk acoustic streaming and pressure nodes. New, biocompatible methods for manipulating microscale objects, such as acoustic microrobots, can also open up new degrees of freedom for studying cellular biology. For example, optical tweezer setups could be replaced with robots to utilize laser setups for other applications, such as the excitation of dyes for super-resolution imaging. Our system utilizes an onboard bubble and is easily added to many biologically relevant systems, requiring only the application of ultrasound with magnetic steering. This bubble is the only thing in the field sensitive enough to the small acoustic field to move, allowing it to be driven to any point in the fluid without the need for labeling or functionalizing particles and cells. This system is also capable of pushing and tweezing in a very small area around the swimmer, allowing it to precisely manipulate cells and particles in crowded environments without damaging cells. The simplicity of this approach, quick fabrication, and low cost also allow for highly complex tasks to be carried out by scientists with any background and training.

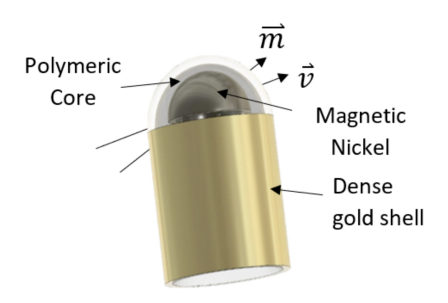


Figure 1. Cross-sectional view of a microrobot, showing all of the components for a functioning swimmer.

#### III. MATERIAL AND METHODS

# A. Fabrication of Microrobots and Operation

Acoustic microrobots were fabricated in four steps. A bullet-shaped polymeric capsule was 3D printed using the Nanoscribe system (Nanofabrication Facility, UPenn). The cavity had a length of 7  $\mu$ m and an inner radius of 2  $\mu$ m. Second, 10 nm of nickel was thermally evaporated onto the substrate with a Kurt Lesker PVD-75 E-beam/Thermal evaporator. Next 40-60 nm of Au was sputtered on the substrate using a Denton Explorer 14 magnetron sputtering system. Finally, surface hydroxyl groups on the gold surface were created using an air plasma for 5 minutes in a Harrick PCD-001-HP, followed by incubation of the substrate in a 75 °C chamber with 20  $\mu$ L of perfluorooctyltrichlorosilane. This created a hydrophobic surface on the robot. Finally, a bake at 100 °C was performed to remove any unreacted silane. Fig. 1 demonstrates the structure of the microrobot.

## B. Experimental Setup

A 1.8 MHz transducer (STEMinc) was fixed to the bottom of a glass microscope slide or silicon wafer and two Kapton polyimide circles were added to the other side, just next to the transducer to allow for use in an inverted microscope. These circles can be used to create a chamber, and scratching the surface of the wafer used to fabricate the microrobots with a pipette tip filled with 7  $\mu$ L of water and transferring that to the chamber gives independent, operational robots that typically operate between 1.0 and 1.6 MHz at 1 Vpp or less (normally 200mVpp), although higher operating voltages are certainly possible. A schematic representation of the experimental design is shown in Fig. 2.

#### C. Bubble-driven Motion

As reported in our previous work [5], this microscale motor operates by trapping a bubble inside a bullet-shaped capsule. The capsule is made dense by addition of the sputter coated gold layer. This ensures that the robot sinks to the bottom of the experimental chamber. Due to the addition of the hydrophobic self-assembled monolayer the capsule can trap a bubble inside itself when added to aqueous media. In the presence of this applied acoustic field, the motor feels a variety of forces that influence its motion, including a

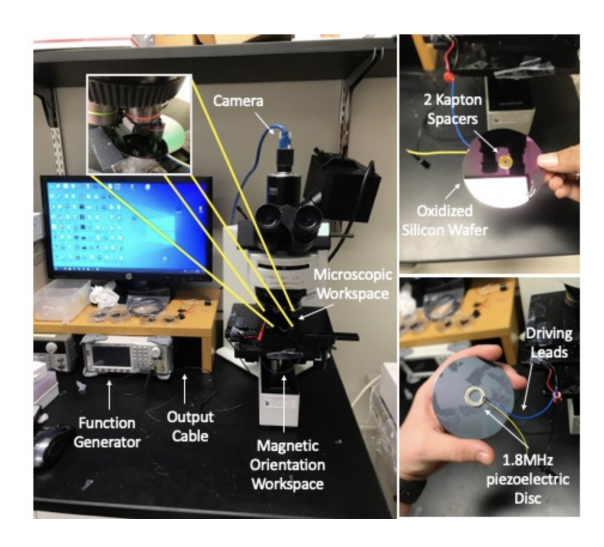


Figure 2. Image of the experimental setup and the chamber is shown, with the transducers highlighted in the lower right panel.

primary  $(F_{SB})$  and secondary Bjerknes force  $(F_{SB})$  and a streaming propulsive force  $F_{SP}$ . The primary Bjerknes force arises when acoustic wave scattering pushes the bubble in the direction of acoustic wave propagation, although we take this term to negligible  $((\frac{F_{SB}}{F_{PB}}\sim 10))$  in this system given the small wave FPB amplitude and the fact that reflected waves propagate towards the motor from many directions. The streaming propulsive  $F_{SB}$ , scales as  $F_{SB} \sim \epsilon^2 \rho_f a^4 f^2$  where a is the radius of the bubble,  $\epsilon$  is the amplitude of oscillation of the bubble,  $\rho_f$  is the density of the fluid and f is the frequency. Finally, due to the presence of a rigid boundary in its vicinity, the microswimmer experiences a secondary Bjerknes force  $F_{SB}$ . The secondary Bjerknes force also arises from acoustic wave scattering, but attracts the motor to the nearest surface because of secondary scattering of the waves off of the very close solid boundary. At the motors resonant frequency, this creates an acoustic reflection of the bubble, which oscillates in phase with the real bubble, pulling the bubble as close to the boundary as possible. This force is what causes the torque which rotates the motor into a vertical direction, with the airwater interface in close proximity to the substrate surface. This force can be expressed as  $F_{SB}\sim -\frac{\rho_f}{4\pi d^2}\langle \dot{V}\rangle^2$  where d is the distance between the bubble and its reflection V is the bubble volume,  $\langle \rangle$  denotes the time average and the dot indicates the time rate of change. The ratio of the secondary Bjerknes force to the streaming propulsive force is  $\frac{F_{SB}}{F_{SP}} \sim 4p(a/d)^2$ . Finally, minute pressure differentials FSP exerted on the bubble by the travelling acoustic wave generate a tambourine-like oscillation at the air-water interface which creates a micro-streaming in the fluid which propels the motor along its long axis away from the open end. The operating frequency of this streaming propulsion depends strongly on the bubbles size [5]. The resonant frequency of a bubble trapped inside a microswimmer can be estimated from equations (1) and (2)

$$f_0 = \frac{1}{2\pi} \left( \frac{\kappa P_0}{\rho (L - L_b) L_b} \right)^{1/2} \mathring{u} M \tag{1}$$

$$M = \left(1 + \frac{4\gamma L_b}{\kappa P_0 a^2}\right)^{1/2} \tag{2}$$

where  $\kappa \sim 1.4$  is the adiabatic index,  $\rho$  is the density of water,  $P_0$  is the pressure in the bubble without the acoustic field,  $L_b$  is the length of the bubble, L is the cavity length, a is the inner radius of the cavity, and  $\gamma \sim 0.07$  N/m is the surface tension of the water-air interface. M must be included to account for the surface tension effect [5]. In addition, increasing the magnitude of this pressure oscillation by raising the transducers voltage, significantly increases the motors speed because the magnitude of the bubble oscillation is larger.

# D. Magnetic Control and Manipulation

As described above, the application of an acoustic field resonant with the bubble rotates the swimmer into a vertical position which poises the robot for motion. In this position, the streaming force is symmetric about the swimmer, yet not enough to overcome the secondary Bjerknes force under low voltage conditions. However, the application of a magnetic field can exert a torque on the motors magnetic components and orient it in a new direction, breaking the symmetry of the vertical stance and propelling the motor in its tilt direction. In our experiments, this is accomplished by rotating a strong handheld magnet and determining the appropriate tilt angles *in operando*. It should be noted that this tilt direction is different for every motor since there is no unified orientation of magnetization.

#### E. Cargo Delivery and Pickup

From this position, the bubble can quickly and precisely be maneuvered to any position within the working field. Also, given the large magnitude of the propulsion force, the swimmers' momentum can be easily transferred to any object in the liquid. By directing the swimmer through the center of mass of an object, that object can be pushed to new positions in the field, although it proves difficult to maintain a straight trajectory without many corrections and re-orientations of the robot. More interestingly and practically, the secondary Bjerknes force can act as an end effector to attach solid objects to the swimmer, just as the swimmer is attracted to the operating surface. This force can be used to grab and drag objects around the field under slightly higher operating voltages (i.e. 800mVpp) and eliminate the need for dynamic corrections that arise with the pushing motion. The object can then be released on command by rotating the motor quickly away from the object or decreasing the operating voltage. For demonstrating the cargo pickup and delivery we used 3 µm polystyrene particles (Sigma Aldrich, USA) as the cargo. A 0.01% concentration of the cargo particles was prepared in ultrapure DI water.

### F. Cellular Manipulation

Human Embryonic Kidney (HEK) cells were used as representative cells for demonstrating cellular manipulation. Frozen (-80 °C) HEK 293FT cell line was purchased from ThermoFisher, USA. The frozen cells were thawed and cultured in Dulbecco's Modified Eagle Medium (DMEM) (ThermoFisher, USA) media containing 10% Fetal Bovine Serum (FBS) (ThermoFisher, USA) and 1% Gibco Geneticin (ThermoFisher, USA) and cultured in the standard cell culture conditions. The cells were used for experiments before they reached 90% confluence. The HEK cells were genetically modified to be fluorescent to check their viability. They were transformed with a plasmid that promotes the constitutive expression of red fluorescent protein (mCherry). The absorption of light for mCherry is in the range of 540-590 nm and emission is in the range of 550-650 nm. The presence of fluorescence in the cells was used as the measure of their viability.

#### IV. RESULTS AND DISCUSSION

# A. Characterization of Robot Motion

The chamber in our setup was filled with 7 µL of 2% w/v solution of the microrobots with ultrapure DI water. Leads from the function generator were connected to a transducer fixed to a silicon wafer, and a glass slide was added above the surface to complete the fluid chamber, as shown in Fig. 2. As the robots have a range of operating frequencies based on the fabrication method, the frequency of the function generator is typically swept from 1.0 to 1.6MHz in 0.01 MHz increments until motion is seen in the form of the motor orienting normally to the substrate. The motors can then be steered with a magnet from below the imaging platform, though this can be altered for unique setups. Imaging was performed on an Olympus BX60M inverted microscope using bright field and darkfield. Videos were captured using a CCD camera, and video processing was performed using FlyCap software. All the images were adjusted for threshold and processed in ImageJ. In the absence of the acoustic field, the robots sink to the bottom of the chamber with their long axis parallel to the substrate, but stand perpendicular to the surface when it is applied. The translational motion of the microrobot can then be initiated upon applying an external magnetic field. The Ni layer on the bullet responds to an external magnetic field in the form of a cylindrical magnetic (45.1 lbs pulling force), which rotates the microrobot, resulting in a net propulsive force in the x-y plane. An experimental demonstration of the self-rotation and translation of microrobots is shown in Fig. 3A and the supporting movie. As shown in this figure, self-rotation of microrobot when the acoustic field is on, and the translation of microrobots over 2 seconds when both acoustic and magnetic fields are applied is shown. Initially, the microrobot orients perpendicular to the substrate with its open end (with the bubble) facing the bottom when the acoustic field is applied. In this position, no translational motion is observed. When a cylindrical magnet (pulling force, 45.1 lbs) is placed next to the fluidic chamber, the microrobot starts to translate in the

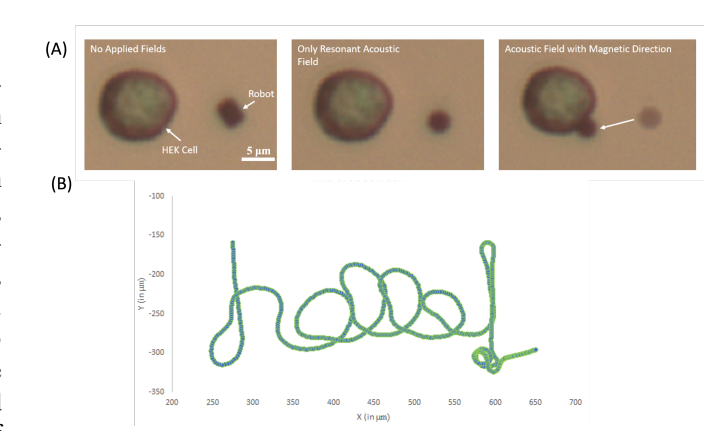


Figure 3. (A) Still images from videos of the self-rotation of microrobots in the presence of acoustic and magnetic field. (B) To demonstrate the precise steering of microrobot, the track of the microrobot spelling 'HELLO!' is shown

direction of its closed end. The direction of movement can be precisely steered by the direction of the magnetic field. The direction of movement can therefore be precisely steered by the direction of the magnetic field to any user-defined location (see supporting movie). Control experiments demonstrated that the microrobots stopped translating immediately when the acoustic field was turned off and that capsules without a trapped air bubble neither self-rotated nor translated in the same acoustic field. Therefore, both the self-rotation and the translational motion of the microrobots are powered by the acoustic field, while the magnetic field acts as a switch to initiate the translational motion by controlling the direction of the streaming propulsive force. In an acoustic field, the motion of the microrobots is sensitive to the applied frequency. Generally, the streaming propulsive force reaches a maximum at the resonant frequency of the bubble. The resonant frequency of a bubble trapped inside a microrobot is different from bubble to bubble in our system due to random variations in bubble length [5]. The use of the applied magnetic field allows the microrobots to be precisely steered. A demonstration of the microrobots in spelling the word 'HELLO' is shown in the accompanying video along with the corresponding track of the particle in Fig. 3B.

### B. Steering Microrobots to Cells

The combination of efficient, precisely directional, and independent propulsion makes the bubble-based microswimmers an ideal tool for selective manipulation of objects. Moreover, their biocompatibility means that they can be easily integrated into cellular environments, especially mammalian cells. For demonstrating the steering of microrobots to mammalian cells 2% w/v solution of the acoustic microrobots was prepared in DMEM.  $5~\mu L$  of the microrobot solution along with  $5~\mu L$  of the HEK cellular solution in DMEM was added to the chamber. As shown in Fig. 4 and the attached video, once the desired cell was located, a microrobot was identified and it was tilted

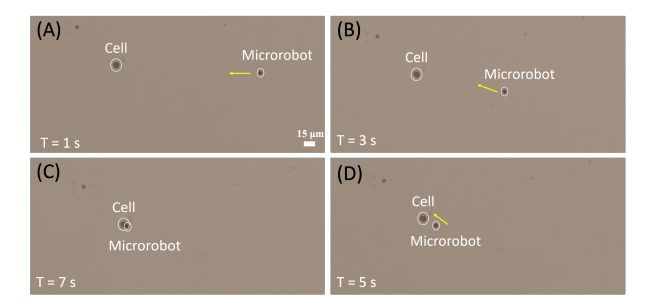


Figure 4. (A)-(D) Still images from the video showing the steering of the microrobot to the cell are shown in progression, clockwise. The cell and microrobot are both outlined and labeled in the still frames. The microrobot can be steered to the cell over 6 seconds.

using the permanent magnet. Then the magnet was used to steer the microrobot to the identified cell.

### C. Cell Manipulation using Microrobots

Generally, cellular manipulation and measurement are performed using either tethered or untethered approaches. Tethered approaches such as the use of micromanipulators or atomic force microscopy (AFM) tips [27] require a continuous connection between the end effector and the cell and thus are not suitable for long-term manipulation of mammalian cells, since they need specific growth environments. On the other hand, untethered techniques like optical tweezers or magnetic fields have low power for efficient manipulation of cells [28]. To overcome these challenges, we demonstrate that acoustic microrobots can be used to rotate and move cells without agitating the medium or surrounding cells. Fig. 5(A) shows a HEK cell ( $\approx 20 \mu m$ ) transported by the microrobot. The microrobot can manipulate the cell using a 'pulling' mode. The pulling mode operates at higher acoustic pressure, at which the microswimmers exhibit strong attractive forces between them and the cells. This attractive force scales approximately as the square of acoustic pressure and thus can overcome the drag force on the cells to pull them with the microrobot, as illustrated in Fig. 5(A). Upon arrival at their new location, the cells could theoretically be released by further tilting the microswimmer to increase the repulsive streaming between them. Due to the size difference between the cell and the microrobot, the robot is also able to rotate the cells by generating a torque in the pushing mode, as shown in Fig. 5(B). The viability of the cell was tested before and after pulling using fluorescence and no change was observed.

#### D. Targeted Cargo Pickup and Delivery using Microrobots

The microrobots can also be used for targeted delivery of payloads to the cells. For a demonstration of cargo pickup and delivery, we combined 2.5  $\mu$ L of microrobots in water with 2.5  $\mu$ L of cargo particle (3  $\mu$ m polystyrene particle) solution. This solution was added to the chamber along with 5  $\mu$ L of HEK cellular solution. The microrobot was able to pick up the cargo due to the 'pulling' mode. Again, this mode operates at slightly

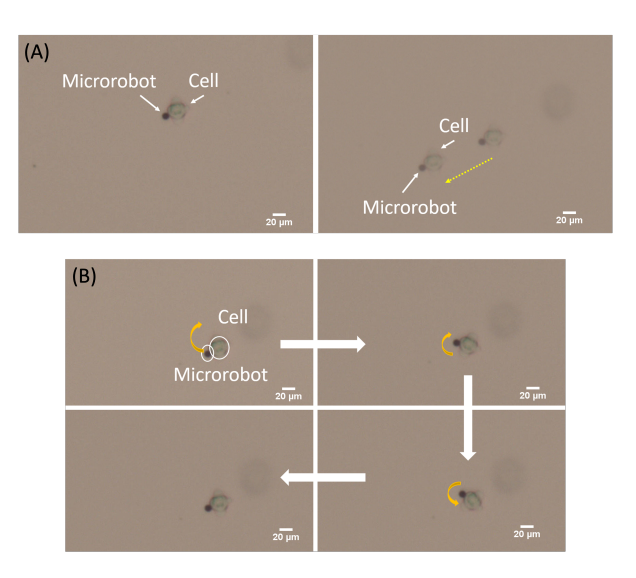


Figure 5. (A) Manipulation of HEK cell using acoustic microrobot is shown. The starting and final position of the microrobot and cell is indicated. The direction of motion is shown by the yellow dashed line. This experimental demonstration was conducted at an acoustic pressure of 1 kPa. (B) Still, images taken from the video demonstrating the rotation of the cell using the microrobot are shown. The direction of rotation is denoted by the yellow arrows. From left to right the cell rotates half-clockwise once and then half counter-clockwise again.

larger acoustic pressure, at which the microrobots exhibit nonnegligible attractive forces on the particles around them. In this situation, the robot can load and transport the cargo particles by moving toward their centers of mass and trapping them via the secondary Bjerknes force. Fig. 6 and the video show a microrobot propelled by a 1 kPa acoustic pressure field and steered to grab only the target particle (highlighted by a white). The microrobot attracts the particle and then steers it across almost the entire diameter of the fluid chamber, which is about 5 mm. The cargo particle is then steered by the microrobot and delivered to a targeted HEK cell. Lastly, the cargo can also be easily released by directing the microrobot away from it.

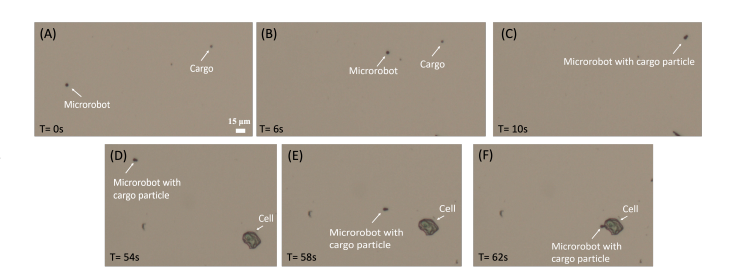


Figure 6. Illustration of the pulling mode of the microrobot for cargo pickup and delivery. (A) Still frames from the video demonstrate that the microrobot (highlighted with the white arrow) can be steered to the cargo particle (labelled). (B) Still frames from the video show that the microrobot drags the cargo particle to the cell. The microrobot and the cargo are labelled with a white arrow and the cellular position is also shown.

### V. CONCLUSION

Here, we demonstrate the utility of using a bubble-powered microswimmer as a microscopic robot for simple, high-speed, bio-compatible cellular manipulation and cargo delivery. We have shown superior control over these microrobots using only a strong handheld magnet and a ceramic transducer driven at biologically relevant ultrasound voltages and frequencies. In addition, we have also demonstrated that our robot can be used for cargo delivery and pickup, which is the main purpose. Our microrobot has a built-in end effector that can pick up and deliver payloads just by a change in voltage or orientation, without prior labeling or functionalization of the cells or particles. This technique opens up a variety of opportunities for biologists and roboticists alike, allowing for quick microscale assembly and manipulation with singeparticle precision. The next goal is to use this technique for a variety of biomedical applications, from interrogations of interesting biological phenomena, to dynamic control of multiple robots via a computer-controlled magnetic field. We imagine this robot and successive nanoscale bubble motors being utilized as cheaper, simpler replacements for intense, field-driven tweezing that could extend the capabilities of many studies and make them more accessible to researchers without the need for expensive, hard-to-use equipment.

#### VI. ACKNOWLEDGMENTS

This work was supported by the National Science Foundation under grant GCR 2219101, CPS 2234869, and the National Health Institute under grant 1R35GM147451. This project was also supported by a grant from the National Institute of General Medical Sciences – NIGMS (5P20GM109021-07) from the National Institutes of Health and the State of Delaware.

#### REFERENCES

- [1] L. Smith, J. C. Kew, X. B. Peng, S. Ha, J. Tan, and S. Levine, "Legged robots that keep on learning: Fine-tuning locomotion policies in the real world," in 2022 International Conference on Robotics and Automation (ICRA). IEEE, 2022, pp. 1593–1599.
- [2] S. Qin, H. Li, and L. Cheng, "A hybrid controller for musculoskeletal robots targeting lifting tasks in industrial metaverse," *IEEE Transactions* on Cybernetics, 2024.
- [3] J. Hwangbo, J. Lee, A. Dosovitskiy, D. Bellicoso, V. Tsounis, V. Koltun, and M. Hutter, "Learning agile and dynamic motor skills for legged robots," *Science Robotics*, vol. 4, no. 26, p. eaau5872, 2019.
- [4] M. Wang, B. Duong, H. Fenniri, and M. Su, "Nanomaterial-based barcodes," *Nanoscale*, vol. 7, no. 26, pp. 11240–11247, 2015.
- [5] L. Ren, N. Nama, J. M. McNeill, F. Soto, Z. Yan, W. Liu, W. Wang, J. Wang, and T. E. Mallouk, "3d steerable, acoustically powered microswimmers for single-particle manipulation," *Science advances*, vol. 5, no. 10, p. eaax3084, 2019.
- [6] S. Das, E. B. Steager, M. A. Hsieh, K. J. Stebe, and V. Kumar, "Experiments and open-loop control of multiple catalytic microrobots," *Journal of Micro-Bio Robotics*, vol. 14, pp. 25–34, 2018.
- [7] Z. Wang, A. Klingner, V. Magdanz, S. Misra, and I. S. Khalil, "Soft bio-microrobots: Toward biomedical applications," *Advanced Intelligent* Systems, vol. 6, no. 2, p. 2300093, 2024.
- [8] A. Elnaggar, S. Kang, M. Tian, B. Han, and M. Keshavarz, "State of the art in actuation of micro/nanorobots for biomedical applications," *Small Science*, vol. 4, no. 3, p. 2300211, 2024.

- [9] C. Dai, Z. Zhang, Y. Lu, G. Shan, X. Wang, Q. Zhao, and Y. Sun, "Robotic orientation control of deformable cells," in 2019 International Conference on Robotics and Automation (ICRA). IEEE, 2019, pp. 8980–8985.
- [10] W. Chen, H. Zhou, B. Zhang, Q. Cao, B. Wang, and X. Ma, "Recent progress of micro/nanorobots for cell delivery and manipulation," Advanced Functional Materials, vol. 32, no. 18, p. 2110625, 2022.
- [11] V. D. Nguyen, J.-O. Park, and E. Choi, "Macrophage-based microrobots for anticancer therapy: Recent progress and future perspectives," *Biomimetics*, vol. 8, no. 7, p. 553, 2023.
- [12] Y. Dai, L. Jia, L. Wang, H. Sun, Y. Ji, C. Wang, L. Song, S. Liang, D. Chen, Y. Feng *et al.*, "Magnetically actuated cell-robot system: precise control, manipulation, and multimode conversion," *Small*, vol. 18, no. 15, p. 2105414, 2022.
- [13] D. Gao, W. Ding, M. Nieto-Vesperinas, X. Ding, M. Rahman, T. Zhang, C. Lim, and C.-W. Qiu, "Optical manipulation from the microscale to the nanoscale: fundamentals, advances and prospects," *Light: Science & Applications*, vol. 6, no. 9, pp. e17 039–e17 039, 2017.
- [14] L.-M. Zhou, Y. Shi, X. Zhu, G. Hu, G. Cao, J. Hu, and C.-W. Qiu, "Recent progress on optical micro/nanomanipulations: structured forces, structured particles, and synergetic applications," ACS nano, vol. 16, no. 9, pp. 13 264–13 278, 2022.
- [15] A. Keloth, O. Anderson, D. Risbridger, and L. Paterson, "Single cell isolation using optical tweezers," *Micromachines*, vol. 9, no. 9, p. 434, 2018
- [16] E. B. Steager, B. Zern, M. S. Sakar, V. Muzykantov, and V. Kumar, "Assessment of protein binding with magnetic microrobots in fluid," in 2013 IEEE International Conference on Robotics and Automation. IEEE, 2013, pp. 5502–5507.
- [17] L.-L. S. Ong, H. Zhu, D. Banik, Z. Guan, Y. Feng, E. L. Reinherz, M. J. Lang, and H. H. Asada, "A robotic microscope system to examine t cell receptor acuity against tumor neoantigens: a new tool for cancer immunotherapy research," *IEEE Robotics and Automation Letters*, vol. 4, no. 2, pp. 1760–1767, 2019.
- [18] Z. Tian, S. Yang, P.-H. Huang, Z. Wang, P. Zhang, Y. Gu, H. Bachman, C. Chen, M. Wu, Y. Xie et al., "Wave number–spiral acoustic tweezers for dynamic and reconfigurable manipulation of particles and cells," *Science advances*, vol. 5, no. 5, p. eaau6062, 2019.
- [19] A. Marzo and B. W. Drinkwater, "Holographic acoustic tweezers," Proceedings of the National Academy of Sciences, vol. 116, no. 1, pp. 84–89, 2019.
- [20] H. Shen, S. Cai, Z. Wang, Z. Ge, and W. Yang, "Magnetically driven microrobots: Recent progress and future development," *Materials & Design*, vol. 227, p. 111735, 2023.
- [21] Y. Feng, M. An, Y. Liu, M. T. Sarwar, and H. Yang, "Advances in chemically powered micro/nanorobots for biological applications: a review," *Advanced Functional Materials*, vol. 33, no. 1, p. 2209883, 2023.
- [22] G. Hwang, A. J. Paula, E. E. Hunter, Y. Liu, A. Babeer, B. Karabucak, K. Stebe, V. Kumar, E. Steager, and H. Koo, "Catalytic antimicrobial robots for biofilm eradication," *Science robotics*, vol. 4, no. 29, p. eaaw2388, 2019.
- [23] S. Kim, S. Lee, J. Lee, B. J. Nelson, L. Zhang, and H. Choi, "Fabrication and manipulation of ciliary microrobots with non-reciprocal magnetic actuation," *Scientific reports*, vol. 6, no. 1, p. 30713, 2016.
- [24] L. Dai, Z. Ge, N. Jiao, J. Shi, and L. Liu, "Manipulation using microrobot driven by optothermally generated surface bubble," in 2019 International Conference on Robotics and Automation (ICRA). IEEE, 2019, pp. 219–224.
- [25] X. Wang, C. Ho, Y. Tsatskis, J. Law, Z. Zhang, M. Zhu, C. Dai, F. Wang, M. Tan, S. Hopyan *et al.*, "Intracellular manipulation and measurement with multipole magnetic tweezers," *Science robotics*, vol. 4, no. 28, p. eaav6180, 2019.
- [26] J.-F. Louf, N. Bertin, B. Dollet, O. Stephan, and P. Marmottant, "Hovering microswimmers exhibit ultrafast motion to navigate under acoustic forces," *Advanced Materials Interfaces*, vol. 5, no. 16, p. 1800425, 2018.
- [27] J. Liu, J. Wen, Z. Zhang, H. Liu, and Y. Sun, "Voyage inside the cell: Microsystems and nanoengineering for intracellular measurement and manipulation," *Microsystems & Nanoengineering*, vol. 1, no. 1, pp. 1– 15, 2015.
- [28] S. Das, E. E. Hunter, N. A. DeLateur, E. B. Steager, R. Weiss, and V. Kumar, "Controlled delivery of signaling molecules using magnetic microrobots," in 2018 international conference on manipulation, automation and robotics at small scales (MARSS). IEEE, 2018, pp. 1–5.